CrossMark

Click for updates

Synthesis and characterization of a new Schiff base derived from 2,3-diaminopyridine and 5-methoxysalicylaldehyde and its Ni(II), Cu(II) and Zn(II) complexes. Electrochemical and electrocatalytical studies

Razika Benramdane[a], Fatiha Benghanem[a], Ali Ourari[a], Saida Keraghel[a] & Gilles Bouet[b]

[a] Faculté de Technologie, Laboratoire d'Electrochimie, d'Ingénierie Moléculaire et de Catalyse Rédox (LEIMCR), Université Sétif-1, Sétif, Algeria

[b] UFR des Sciences Pharmaceutiques et d'Ingénierie de la Santé, Laboratoire SONAS EA 921, SFR QUASAV 4207, UNAM, Université d'Angers, Angers Cedex 01, France
Accepted author version posted online: 06 Dec 2014.Published online: 02 Jan 2015.

PLEASE SCROLL DOWN FOR ARTICLE

Taylor & Francis
Taylor & Francis Group

Synthesis and characterization of a new Schiff base derived from 2,3-diaminopyridine and 5-methoxysalicylaldehyde and its Ni(II), Cu(II) and Zn(II) complexes. Electrochemical and electrocatalytical studies

RAZIKA BENRAMDANE†, FATIHA BENGHANEM†, ALI OURARI†, SAIDA KERAGHEL† and GILLES BOUET*‡

†Faculté de Technologie, Laboratoire d'Electrochimie, d'Ingénierie Moléculaire et de Catalyse Rédox (LEIMCR), Université Sétif-1, Sétif, Algeria
‡UFR des Sciences Pharmaceutiques et d'Ingénierie de la Santé, Laboratoire SONAS EA 921, SFR QUASAV 4207, UNAM, Université d'Angers, Angers Cedex 01, France

We describe the synthesis and characterization of a new tetradentate Schiff base ligand obtained from 2,3-diaminopyridine and 5-methoxysalicylaldehyde. This ligand (H_2L) reacted with nickel(II), copper(II), and zinc(II) acetates to give complexes. The ligand and its metal complexes were characterized using analytical, spectral data (UV–vis, IR, and mass spectroscopy), and cyclic voltammetry (CV). The crystal structure of the copper complex was elucidated by X-ray diffraction studies. The electrochemical behavior of these compounds, using CV, revealed that metal centers were distinguished by their intrinsic redox systems, *e.g.* Ni(II)/Ni(I), Cu(II)/Cu(I), and Zn(II)/Zn(I). Moreover, the electrocatalytic reactions of Ni(II) and Cu(II) complexes catalyze the oxidation of methanol and benzylic alcohol.

Keywords: Tetradentate Schiff base; Metal complexes; Crystal structure; Cyclic voltammetry; Electrocatalytic oxidation

1. Introduction

Porphyrinic and macrocyclic ligands have been extensively studied in coordination chemistry [1–3] due to their chelating properties allowing them to selectively coordinate metal ions

---

*Corresponding author. Email: gilles.bouet49@orange.fr

[4–7]. Their coordination reactions with transition metals lead to formation of an important variety of complexes currently involved in several applications. Schiff base ligands are also well known for their complexing properties [8]. These ligands have received much attention during the last decades for their potential applications as catalysts for olefin epoxidation or hydrocarbon oxidation [9, 10] and their biological activities such as antimicrobial, antitumoral, and anti-inflammatory properties [11, 12]. Thus, these compounds may also be involved in the catalytic model systems of cytochrome P450 in which they are used as catalysts in biomimetic oxidation reactions of olefins and hydrocarbons [9, 10]. Schiff bases derived from diaminopyridine and salicylaldehyde were relatively less described in the literature [13], in spite of their excellent performance as efficient catalysts for reduction or oxidation reactions. As a continuation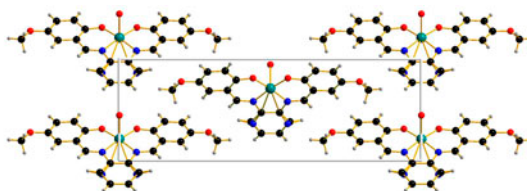 of our recent papers [14] we describe here the synthesis and characterization of a Schiff base obtained from 2,3-diaminopyridine and 5-methoxysalicylaldeyde and its complexes with Ni(II), Cu(II), and Zn(II). They have then been tested as electrocatalysts to electrochemically oxidize methanol and benzylic alcohol. The reaction pathway leading to these compounds is given in scheme 1.

2. Experimental

2.1. *Physical measurements*

All chemicals used for the syntheses and measurements were of analytical reagent grade (Aldrich) and used as received. The solvents were dried before use with appropriate drying agents. The conductivities of complexes Ni(II)-L (**1**), Cu(II)-L (**2**), and Zn(II)-L (**3**) were measured using DMF solutions containing 10^{-3} M of complex. ^{1}H NMR spectra were recorded with a Bruker AC 300 at 25 °C using CDCl$_3$ as solvent and tetramethylsilane as
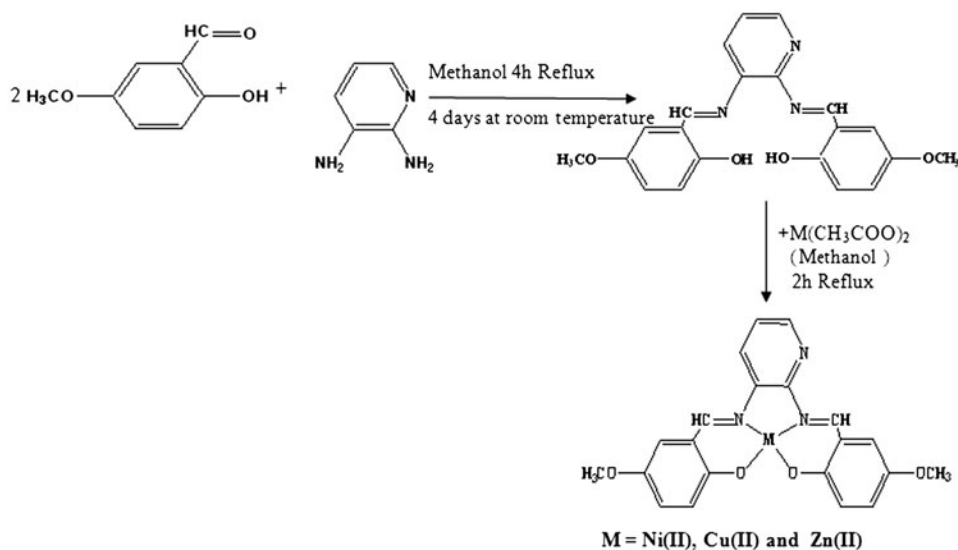
Scheme 1.

internal reference; chemical shifts are given in ppm. IR spectra were recorded on a Perkin Elmer 1000-FT-IR Spectrometer using KBr disks. Electronic spectra were obtained on a Unicam UV-300 Spectrophotometer (1 cm path length cell) in DMF solutions. Microanalyses (table 1) were performed on "Microanalyser Flash EA1112CHNS Thermoelectron" (Laboratoire des Sciences Chimiques, Rennes-1 University, France). Electrochemical experiments were performed at 25 °C on Voltalab 40 Potentiostat Galvanostat controlled by a microcomputer. The cyclic voltammograms were recorded after compilation of electrochemical data, obtained with an individual 5 mL cell using a conventional three-electrode system in DMF solutions with a 0.1 M ionic strength (tetra-*n*-butylammonium hexafluorophosphate; Bu_4NPF_6) and ligand or complex 0.001 M. The electrodes were polished using diamond paste and rinsed with acetone and then DMF. Working electrode was a glassy carbon disk (2 mm diameter), the counter electrode was a platinum wire, and the reference electrode was a saturated calomel electrode (SCE).

2.2. *Crystal data collection and processing*

The crystal of $[C_{21}H_{17}N_3O_4Cu \cdot H_2O]$ is orthorhombic with *Pmn2₁* space group. The crystal data and instrumental parameters used in the unit-cell determination and data collection are given in table 2. X-ray single-crystal diffraction data were collected at 296 K on a Bruker APEX II CCD diffractometer equipped with a graphite monochromator using Mo K$_\alpha$ radiation (λ = 0.71073 Å). The structure was solved by direct methods using the SIR2002 program [15] and refined on F^2 by full matrix least-squares [16]. Unit cell refinement using all observed reflections and data reduction were performed using SAINT. All nonhydrogen atoms were refined anisotropically and the hydrogens were included in geometric positions but not refined.

2.3. *Synthesis of H₂L*

2.3.1. H₂L was prepared according to the literature [17]. To 5-methoxy-2-hydroxybenzaldehyde (608 mg, 4 mM) in MeOH (8 mL), was slowly added, 2,3-diaminopyridine (220 mg, 2 mM) in MeOH (8 mL). This mixture was refluxed with constant stirring under nitrogen for 4 h. After cooling, the precipitate was recovered by filtration and washed several times with methanol and finally diethyl ether.

Table 1. Analytical data for *H₂L*, **1**, **2**, and **3**.

Compound	Color	Yield (%)	M.p. (°C)	Λ_M (Ω^{-1} cm^2 M^{-1})	Elemental Anal. Calcd (Found) (%)		
					C	H	N
$C_{21}H_{17}N_3O_4$ (*H₂L*)	Yellow	74	128	08.44	66.83 (66.42)	5.07 (5.11)	11.13 (11.20)
$C_{21}H_{17}N_3O_4Ni \cdot H_2O$ (**1**)	Brown	77	>300	22.91	55.79 (54.88)	4.24 (4.12)	9.29 (9.29)
$C_{21}H_{17}N_3O_4Cu \cdot H_2O$ (**2**)	Green	70	>300	22.94	55.20 (54.78)	4.19 (4.12)	9.20 (9.17)
$C_{21}H_{17}N_3O_4Zn \cdot H_2O$ (**3**)	Orange	80	>300	14.83	54.98 (54.80)	4.17 (4.13)	9.16 (8.98)

Table 2. Crystallographic data for **2**.

Formula	$[Cu(C_{21}H_{17}N_3O_4) \cdot H_2O]$
Formula weight	456.93
Crystal system	Orthorhombic
Space group	$Pmn2_1$
a (Å)	23.162(7)
b (Å)	5.0997(14)
c (Å)	7.769(2)
V (Å^3)	917.7(4)
Z	2
D_{Calcd} (g cm^{-3})	1.654
Crystal size (mm)	$0.12 \times 0.06 \times 0.04$
Absorption coefficient (mm^{-1})	1.232
$F(0\,0\,0)$	470
h, k, l limits	$-33 \leq h \leq 32$
	$-7 \leq k \leq 7$
	$-11 \leq l \leq 11$
Reflections collected/unique	10,836/3028 [$R_{int} = 0.0589$]
Data $I > 2\sigma(I)$/restraints/parameters	2385/149/6
θ_{min}, θ_{max}	1.76, 31.50
Goodness-of-fit on F^2	0.957
R_1	0.0398, 0.0895
wR_2 [$I \geq 2\sigma(I)$]	0.0538, 0.1089

^{1}H NMR: δ-Chemical shifts in ppm: δOH(1H, s = 12.95); δOH(1H, s = 12.40); δHC = N (1H, s = 9.50); δHC = N(1H, s = 8.60); δH$_{\alpha(pyridine)}$(1H, d = 8.40); δH$_{arom.}$(8H, m = 7.60–6.85, centered at 7.22); δCH$_3$O(6H, s = 3.82). Mass spectra: molecular peak (M$^+$) m/z 378.148 (100%), [M$^+$ + 1H$^+$] m/z 379.151 (20%), [M$^+$ + 2H$^+$] m/z 380.153 (2.85%).

2.4. *Synthesis of the complexes*

Complexes **1**–**3** were prepared according to this general procedure. Hydrated metal acetate (2 mM; 10 mL MeOH) was added dropwise to H_2L (2 mM; 5 mL MeOH). After refluxing with stirring under nitrogen atmosphere for 2 h, the mixture was left at room temperature and a precipitate was formed. It was filtered, washed several times with small amounts of MeOH, previously flushed with nitrogen, and finally dried in vacuum. The purity of these compounds was checked by TLC (silica gel plates, solvent: CH$_2$Cl$_2$/MeOH mixture 9.5/0.5, v/v).

The main analytical data for the ligand and the complexes are given in table 1.

3. Results and discussion

The ligand (L) and its metal complexes: M(II)-L, M = Ni(II), Cu(II), and Zn(II) were characterized using physicochemical techniques such as UV–vis, FT-IR (table 3), elemental analysis, and cyclic voltammetry (CV). The elemental analysis and main physical characteristics of the ligand and its complexes are summarized in table 1. The ^{1}H NMR and mass spectral analyses demonstrated only the molecular structure of the ligand. In addition, the crystal structure of the copper(II) complex **2** was elucidated using single-crystal X-ray diffraction analysis.

Table 3.   Main spectroscopic data for the ligand and its complexes.

Compound	Infrared (cm^{-1})					UV–vis (DMF solution)	
	$v(C=N_{Im})$	$v(C=N_{Pyr})$	$v(C–O)$	$v(M–O)$	$v(M–N)$	λ_{max} (nm)	ε (l M^{-1} cm^{-1})
H_2L	1629	1584	1273	–	–	276	73,175
						319	62,775
1	1628	1563	1248	452	515	270	72,268
						386	55,182
						512	21,345
2	1594	1562	1244	490		272	65,885
						327	59,742
						458	44,650
3	1597	1563	1246	417	550	281	70,230
						315	83,695
						443	69,983

3.1. *Molar conductivity*

H_2L Λ_M molar conductivity is 8.44 Ω^{-1} cm^2 M^{-1} (table 1) and those of **1–3** are higher showing the nonionic state of the ligand. The conductivities of Ni(II) and Cu(II) complexes are 22.94 and 22.91 Ω^{-1} cm^2 M^{-1}, respectively, while in the case of zinc complex this value is lower (14.83 Ω^{-1} cm^2 M^{-1}), due to its d^{10} electronic configuration. These values express the ionic character of the complexes.

3.2. *Crystal structure of [CuL·H$_2$O] (2)*

3.2.1. Molecule description. The symmetrical unit contains ½ molecule of complex and the total molecule is generated by a symmetry (figure 1) where the ligand acts as a diphenolate anion. The pyridine nitrogen is exchanged by C10, so that in each position there is simultaneously 50% of N and 50% of C10. The copper(II) ion is five-coordinate, linking to N-imino, O from hydroxylate, and finally to water in apical position.

The ligand is planar and the highest deviations to this plane are observed with hydrogens of the methyl groups (0.9825 Å for H1C for example) and of the pyridine ring (H10A: 0.2959 Å).

The C8–N1 bond (table 4) with a 1.295(4) Å length is typical of a carbon–nitrogen double bond while the C9–N1 bond length is 1.413(4), corresponding to a single bond. Around
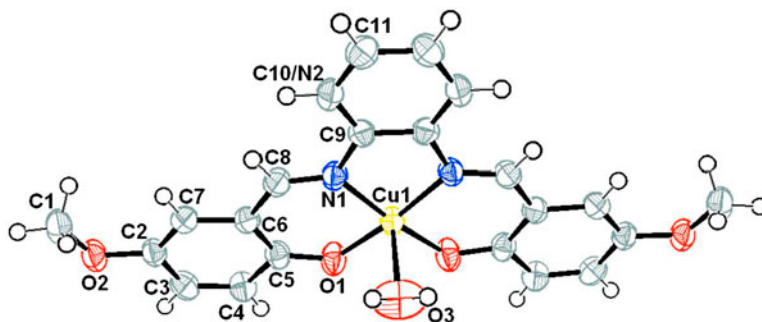

Figure 1.   ORTEP view (50% ellipsoids) of copper complex (**2**) and numbering scheme.

Table 4.   Selected bond lengths (Å) and angles (°) for **2**.

Bond distances (Å)		Bond angles (°)	
Cu1–O1	1.9133(22)	O1–Cu1–O1$^{\#}$	88.90(8)
Cu1–N1	1.9586(24)	O1$^{\#}$–Cu1–N1$^{\#}$	93.47(6)
Cu1–O3	2.4361(38)	O1$^{\#}$–Cu1–N1	173.28(7)
C8–N1	1.2948(38)	O1–Cu1–O3	94.28(7)
C9–N1	1.4129(39)	N1$^{\#}$–Cu1–O3	91.82(7)
		O1–Cu1–N1$^{\#}$	173.28(7)
		O1–Cu1–N1	93.47(6)
		N1$^{\#}$–Cu1–N1	83.50(9)
		O1$^{\#}$–Cu1–O3	94.28(7)
		N1–Cu1–O3	91.82(7)

$^{\#}$Symmetry code: −x, y, z.

Cu(II), the bond lengths are 1.9133(22) Å for Cu1–O1 and 1.9586(24) Å for Cu1–N1. However, the Cu1–O3 bond (water) is longer: 2.4361(38) Å. The angles are close to 90°, with the smallest value for N1–Cu–N1# of 83.50°.

3.2.2. Crystal packing. The crystal packing is made of alternate layers along the [0 0 1] plane, with a 59.06° angle between them (figure 2). This structure is stabilized through hydrogen bonds (table 5), one intramolecular C–H⋯N, and two intermolecular C–H⋯O and O–H⋯O hydrogen bonds (figure 3). The crystal is further stabilized by C–H π interactions and π–π stacking (shortest centroid-to-centroid distance 3.799(8) Å with interplanar distance of 3.469(2) Å).

3.3. *Infrared spectra*

The main infrared bands are reported in table 3. The infrared spectrum of the ligand shows a broad band at 3450 cm^{-1}, attributed to v(C–OH), for intra- and intermolecular hydrogen bonds for hydroxyl group. The characteristic vibration band at 1629 cm^{-1} was assigned to
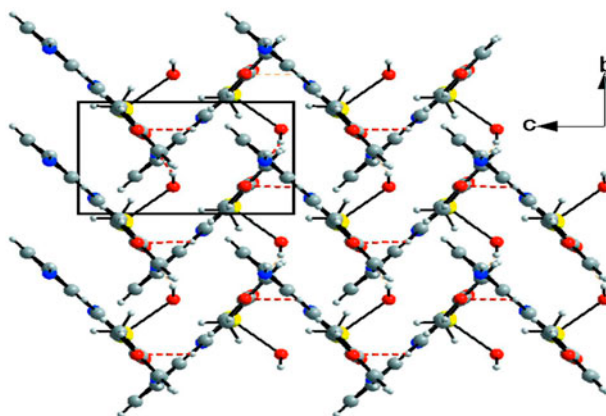

Figure 2.   Crystal packing of **2** along the *a* axis.

Table 5. Geometrical parameters for hydrogen bonds.

D–H···A	D–H (Å)	H···A (Å)	D···A (Å)	D–H···A (°)
O3–H1W···O[i]	0.84(2)	2.19(2)	2.993(3)	146(2)
C8–H8*A*···O2[ii]	0.93	2.57	3.330(3)	139
C8–H8*A*···N2	0.93	2.49	2.844(3)	103
C1–H1*B*···Cg[iii]	0.96	2.71	3.528(4)	143

Symmetry codes: (i) $-x, y + 1, z$; (ii) $-x - 1/2, -y + 2, z + 1/2$; (iii) $-x + 3/2, -y + 2, z + 1/2$.
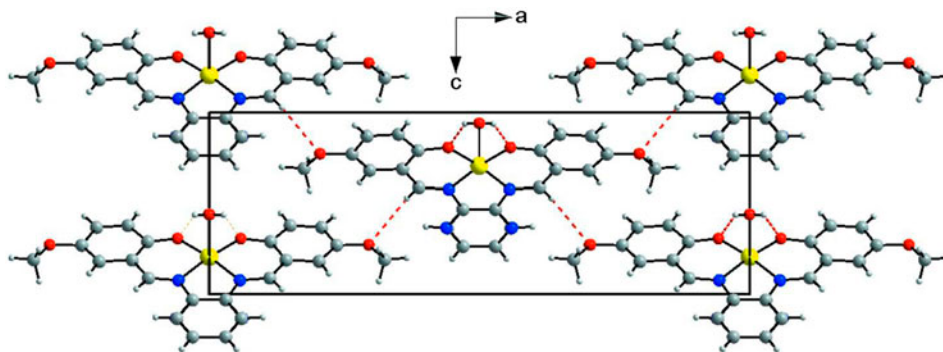

Figure 3.   Crystal packing of **2** along the *b* axis with intermolecular hydrogen bonds (dashed lines).

the stretching vibration of the azomethine group v(C=N). The following absorption bands in the 1600–1430 cm^{-1} region correspond to v(C=C) vibrations of the aromatic ring, while those observed between 1300 and 950 cm^{-1} are currently ascribed to vibration of the ether function [18].

In spectra of the complexes, v(C–OH) bands of phenolic groups are absent. However, bands in this region are due to coordination water as described in the crystal structure of **2** [19]. The azomethine vibration is shifted from 1629 to 1594 cm^{-1} indicating a bathochromic effect, due to an important electronic delocalization through the coordinated metal [20, 21]. This result may be again supported by ether v(C–O) bands shifting to higher wavenumbers (1156–1273 cm^{-1}) expressing a strengthening of their electronic density from the coordinated metal. Some new bands v(M–O) and v(M–N) due to coordination are observed as well [22, 23]. Therefore, both these frequencies are, respectively, located at 417 and 550 cm^{-1} for Ni(II)-L (**1**). Moreover, these absorption bands are observed at 452 and 515 cm^{-1} for Cu(II)-L (**2**) and only at 450 cm^{-1} for Zn(II)-L (**3**) [22, 23].

3.4. *Electronic spectra*

The electronic spectrum of H_2L shows two absorptions (table 3). The first at 276 nm was attributed to π–π* transitions while the second, very large, observed at 319 nm, was ascribed to n–π* transitions. Electronic spectra of the complexes exhibit three absorptions with those appearing between 270 and 386 nm attributed to the π–π* and n–π* transitions of the ligand as already reported [24]. The third arises from coordination of the metal to the ligand as discussed in the IR spectra section. This absorption known as the "Soret-band" at 400–450 nm is informative, characterizing metal coordination to porphyric ligands [25].
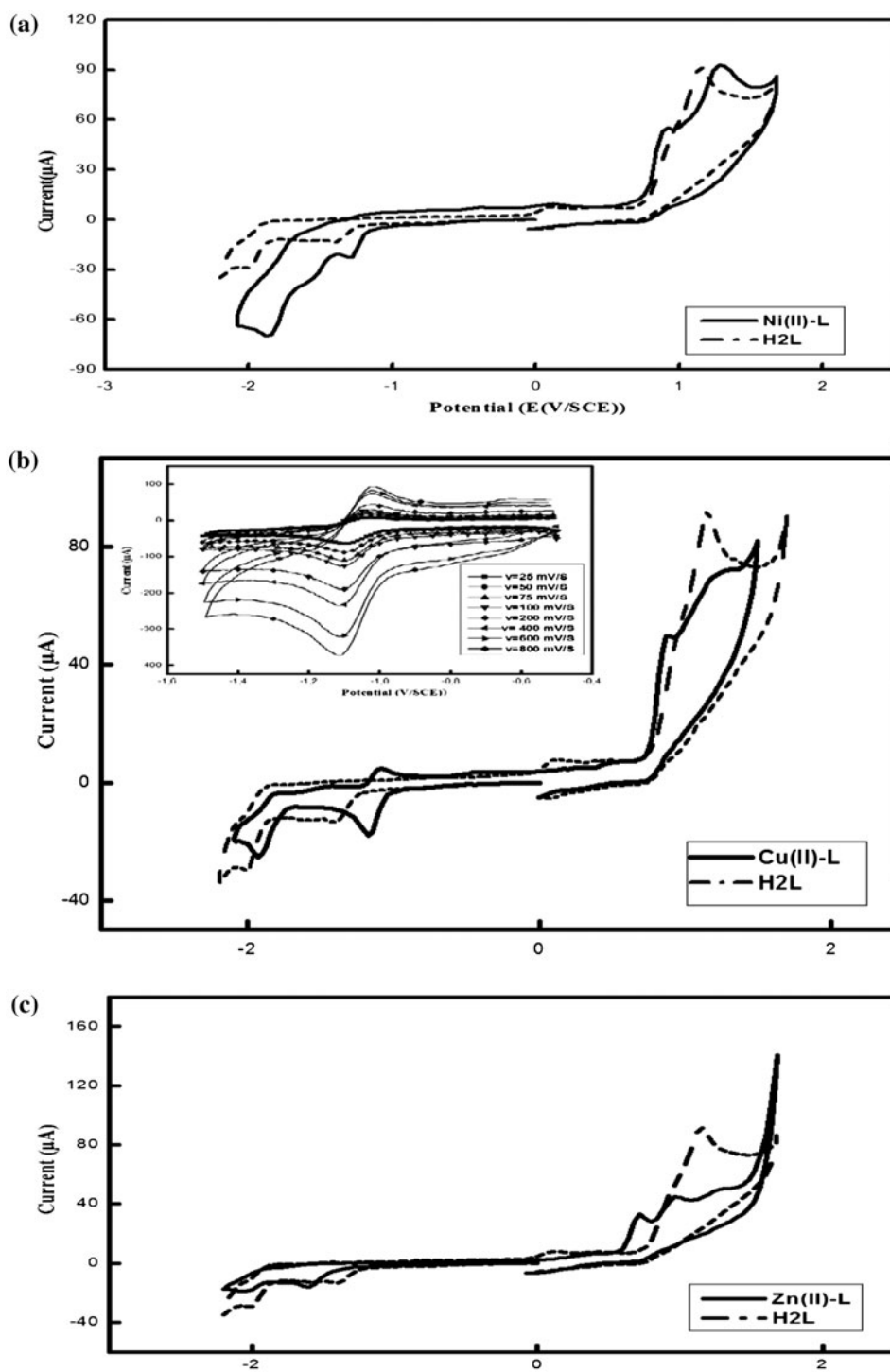
Figure 4. Cyclic voltammograms in DMF, $C = 0.001$ M, $\mu = 0.1$ M (Bu$_4$NPF$_6$), scan rate 25 mV s^{-1}. (a) **1** (solid line) and H_2L (dashed line); (b) **2** (solid line) and H_2L (dashed line); (c) **3** (solid line) and H_2L (dashed line).

This corresponds to the intense absorption bands observed in the spectra of **1–3** at 512, 458, and 443 nm, respectively. The nickel complex (**1**) shows a broad peak at 512 nm and its lower molar absorptivity is characteristic for d–d transitions [26, 27].

3.5. *Structures of 1 and 3*

Starting from the crystal structure of **2** and taking into account the infrared and electronic spectra, we propose the same structure for the three complexes in which the Schiff base coordinates through O of phenolate and N of imino.

3.6. *Electrochemical study*

3.6.1. Electrochemical properties. The redox behaviors of the ligand and its complexes were investigated by CV in DMF. This study was performed from −2100 to +1700 mV/SCE. The four compounds show two reduction waves between −1400 and −2050 mV/SCE for the cathodic potentials. For anodic potentials, one oxidation wave was observed for the ligand and two oxidation waves for **1** and **2**. The zinc complex shows a different behavior with three oxidation waves.

3.6.2. Ligand (H$_2$L). The cyclic voltammogram of the ligand (figure 4, curve A) shows two reduction waves. The first is located at $E_{pc1} = -1405$ mV/SCE and assigned to the reduction of the pyridinic moieties while the second is observed at $E_{pc2} = -2008$ mV/SCE and attributed to the reduction of azomethine. Both these waves are irreversible. At the anodic side, only one oxidation wave was observed at $E_{pa1} = +1148$ mV/SCE, indicating the oxidation of phenolic groups.

Figure 5. Cyclic voltammograms (0.001 M in 0.1 M Bu$_4$NPF$_6$ DMF solution scan rate 25 mV s^{-1}) for the electro-catalytic oxidation of methanol: Inset (A): **1**, methanol concentrations: (a) 0.0 M, (b) 0.0097 M, (c) 0.0437 M, (d) 0.160 M, (e) 0.2377 M. Inset (A′): dependence of oxidation peak current *versus* methanol concentration. Inset (B): **2**, methanol concentrations: (a) 0.0 M, (b) 0.049 M, (c) 2.91 M, (d) 7.26 M, (e) 12.11 M, (f) 25.2 M. Inset (B′): dependence of oxidation peak current *versus* methanol concentration.
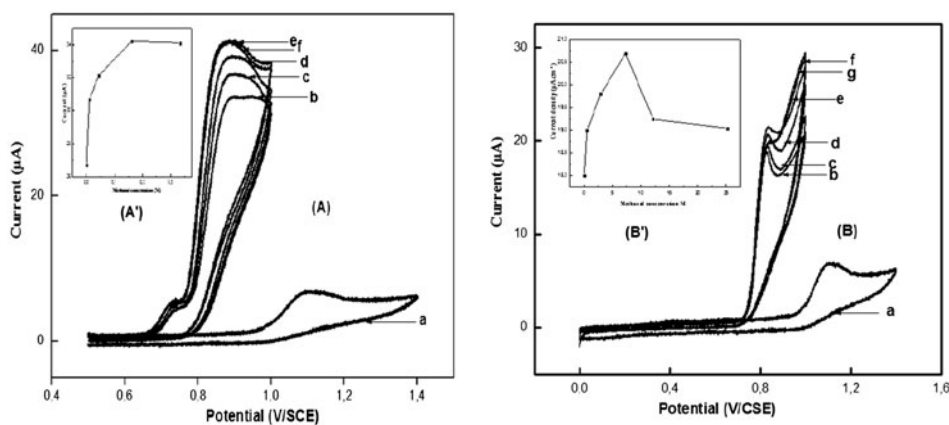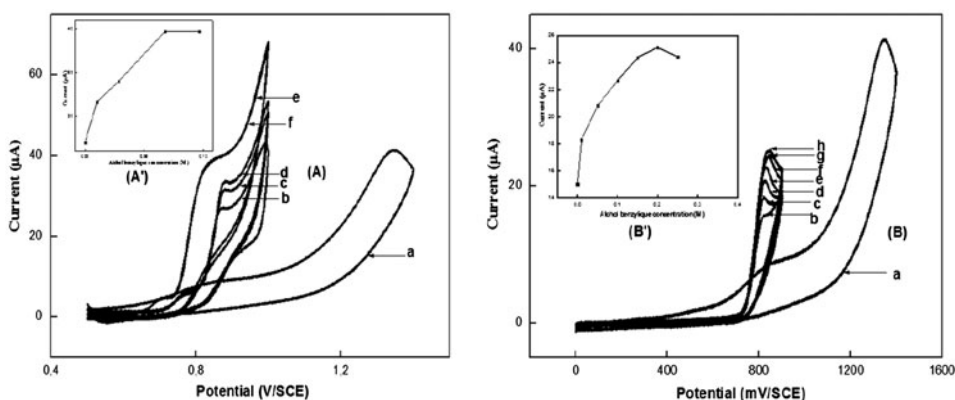
Figure 6. Cyclic voltammograms (0.001 M in 0.1 M Bu_4NPF_6 DMF solution scan rate 25 mV s^{-1}) for the electro-catalytic oxidation of benzylic alcohol: Inset (A): **1**, benzylic alcohol concentrations: (a) 0.0 M, (b) 0.0039 M, (c) 0.0346 M, (d) 0.08114 M, (e) 0.116 M. Inset (B): dependence of oxidation peak current *versus* benzylic alcohol concentration. Inset (A'): **2**, benzylic alcohol concentrations: (a) 0.0 M, (b) 0.01 M, (c) 0.05 M, (d) 0.11 M, (e) 0.15 M, (f) 0.2 M, (g) 0.25 M. Inset (B'): dependence of oxidation peak current *versus* benzylic alcohol.

3.6.3. Nickel complex (1). Cyclovoltammogram of **1** (figure 4, curve A) shows two reduc-tion waves located at $E_{pc1} = -1294$ and $E_{pc2} = -1865$ mV/SCE, respectively. The first was attributed to reduction of Ni(II) to Ni(I) [30], while the second is assigned to reduction of the azomethine. During the back sweep, two oxidation waves were observed at $E_{pa1} = +927$ and $E_{pa2} = +1294$ mV/SCE. The first one was ascribed to oxidation of Ni(II)–Ni(III), whereas the second expresses the oxidation of the ligand as reported above. The redox sys-tems of M(II)/M(I) and M(III)/M(II) generally observed for both Cu and Ni revealed that the nickel complex is not reversible, while the copper complex shows a reversible system for the first redox couple and an irreversible one for the second.

3.6.4. Copper complex (2). Cyclovoltammogram of the copper complex (figure 4, curve B) shows two reduction waves at $E_{pc1} = -1169$ and $E_{pc2} = -1922$ mV/SCE, respectively. The first was attributed to reduction of Cu(II)–Cu(I) [28], while the second is ascribed to reduction of azomethine. Along the back sweep, an oxidation wave appearing at $E_{pa1} = -1083$ mV/SCE expresses the reoxidation of Cu(I)–Cu(II). This redox system ($E_{pc1} = -1169$, $E_{pa1} = -1083$ mV/SCE) was quasi-reversible [29, 30]. Two additional oxidation waves were observed at $E_{pa2} = +884$ and $E_{pa3} = +1275$ mV/SCE. The first one was assigned to oxidation of Cu(II)–Cu(III), whereas the second is due to oxidation of the ligand. The redox couple Cu(II)/Cu(III) is not reversible.

3.6.5. Zinc complex (3). At cathodic potentials, the cyclovoltammogram of **3** is almost identical to that of H_2L as illustrated in figure 4 (curve C). The exceptions are some dis-placements of certain waves, namely the first reduction wave appearing at $E_{pc1} = -1405$ for the ligand and $E_{pc1} = -1603$ mV/SCE for **3**. This shift of -200 mV may be explained by an excess of electronic delocalization due to coordination of the metal. At anodic potentials, three oxidation waves are observed without any presence of zinc redox couple.

3.7. *Electrocatalytical study*

The Ni(II) and Cu(II) complexes show electrocatalytic activities toward oxidation of methanol and benzylic alcohol as described below.

3.7.1. Complex 1 catalyst for oxidation. Figure 5 shows the oxidation of methanol. When the molecule is used as substrate without any catalyst, its oxidation wave is observed at more anodic potentials (1113 mV/SCE) while in the presence of catalyst, the oxidation wave is significantly shifted to less anodic potentials (919 mV/SCE). Thus, the resulting difference in potential values is 194 mV indicating that the oxidation of methanol is an electrocatalytic reaction. These electrocatalytic processes of small molecules have been extensively studied [31–33]. On figure 5, we observe progressive increase in Ni(III)/Ni(II) redox system i_{pa} for which the i_{pc} peak current was not observed. When the concentration effect was investigated (figure 5, curve A), we note a continuous enhancement of the oxidation wave when methanol concentration increased until reaching a plateau for a 0.160 M concentration, indicating that all catalytic sites are saturated (figure 5, curve A′). This figure shows the effect of methanol concentration on the anodic peak current. As methanol concentration increases, the peak height (i_{pa}) increases linearly with methanol concentrations up to 0.160 M. At low methanol concentrations, we assume that this increase in the peak height (i_{pa}) indicated that methanol oxidation is controlled by a diffusion process [33]. Therefore, as the methanol concentration increased, the rate of oxidation seems to be limited by the catalytic process, and its rate depends on the reaction between methanol and Ni(III) species [34–36].

For the oxidation of benzylic alcohol, the same catalyst was used in identical electrocatalytic conditions and the same electrocatalytical behavior as for methanol oxidation is produced as shown in figure 6 (curve A). The electrocatalytical behavior for the oxidation of benzylic alcohol was similar to methanol oxidation. The difference between the oxidation waves of benzylic alcohol (with and without) catalyst was estimated at 436 mV (figure 6, curve A). This synthesis is attractive due to its applications in pharmaceutical and agrochemical processes [37–39]. On figure 6 (curve A), the increasing of the i_{pa} peak current was accompanied by a significant shifting of the oxidation wave potential from +0.850 to +0.775 V/SCE, indicating an electrocatalytic effect [40]. The concentration is quite similar to the behavior of methanol oxidation, showing continuous increasing of the i_{pa} peak current until reaching a pseudo-plateau as earlier observed for methanol oxidation (figure 6, curve A′).

3.7.2. Complex 2 catalyst for oxidation. Methanol oxidation was also carried out using **2** as catalyst. In this case, an irreversible anodic wave was observed at 0.83 V/SCE. Progressive adding of methanol leads to continuous increasing of the i_{pa} peak current up to 7.26 M (figure 5, curve B). A further addition of methanol induces an important decrease in the anodic peak current (i_{pa}), suggesting a partial loss of the electrocatalytic activity. This decreasing of the electrocatalytic activity with copper complex (figure 5, curve B′) was rather explained as stability for the nickel catalyst.

The same cyclovoltammogram shape was observed when the effect of the concentration was investigated using **1** as electrocatalyst to oxidize benzylic alcohol, with an irreversible anodic wave. Successive additions of benzylic alcohol show a continuous increasing of the i_{pa} peak current as illustrated in figure 6 (curve B). The next adding of substrate causes a slight decrease as previously observed for methanol oxidation (figure 6, curve B′).

4. Conclusion

A Schiff base ligand and its Ni(II), Cu(II), and Zn(II) complexes were synthesized and characterized by routine physicochemical methods including electrochemistry. The crystal structure of the Cu(II) complex was determined, showing that Cu(II) is coordinated through two phenolate oxygens and two imine nitrogens from the tetradentate Schiff base anion in a distorted square-pyramidal geometry. Electrochemical properties of H_2L and its metal complexes were investigated pointing out the M(II)/M(I) and M(III)/M(II) redox systems for copper and nickel. The nickel complex is not reversible while the copper complex has a reversible system for the first and an irreversible redox couple for the second. These two compounds developed good electrocatalytic properties to oxidize methanol and benzylic alcohol. A basic medium is appropriated for these oxidation reactions, since the alcoholate species are more easily oxidized than the corresponding neutral alcohol. Thus, in spite of catalytical properties of some transition metal complexes recently reported [41–46], our catalysts oxidize the two alcohols at relative low potential values suggesting high selectivity and stability in mild experimental conditions of temperature and pressure, in a heterogeneous catalytic system, where the modified electrodes containing catalytic species may be used as very efficient catalysts [47].

References

[1] (a) R.A. Sheldon, J.K. Kochi. *Metal Catalysed Oxidation of Organic Compounds*, Academic Press, New York, NY (1981); (b) A.E. Martel, D.T. Sawyer, Oxygen complexes and oxygen activation by transition metals. In *Proceedings of Fifth Annual IUCCP Symposium*, Plenum, New York (1988).

[2] (a) H. Mimoun. In *Comprehensive Coordination Chemistry*, G. Wilkinson, R.D. Gillard, J.A. Mc Clevert (Eds), Vol. 6, pp. 317–410, Pergamon Press, Oxford (1987); (b) R.S. Drago. *Coord. Chem. Rev.*, **117**, 185 (1992).

[3] (a) K. Wichmann, B. Antonioli, T. Söhnel, M. Wenzel, K. Gloe, J.R. Price, L.F. Lindoy, A.J. Blake, M. Schröder. *Coord. Chem. Rev.*, **250**, 2987 (2006) ; (b) S.J. Archibald. *Annu. Rep. Prog. Chem. Sect. A*, **103**, 264 (2007); (c) C. Bazzicalupi, A. Bencini, A. Bianchi, A. Danesi, E. Faggi, C. Giorgi, S. Santarelli, B. Valtancoli. *Coord. Chem. Rev.*, **252**, 1052 (2008).

[4] R.M. Izatt, J.S. Bradshaw, S.A. Nielsen, J.D. Lamb, J.J. Christensen, D. Sen. *Chem. Rev.*, **85**, 271 (1985).

[5] R.M. Izatt, K. Pawlak, J.S. Bradshaw, R.L. Bruening. *Chem. Rev.*, **91**, 1721 (1991).

[6] R.M. Izatt, K. Pawlak, J.S. Bradshaw, R.L. Bruening. *Chem. Rev.*, **95**, 2529 (1995).

[7] K. Choi, A.D. Hamilton. *Coord. Chem. Rev.*, **240**, 101 (2003).

[8] B. Meunier. *Chem. Rev.*, **92**, 1411 (1992).

[9] K. Srinivasan, P. Michaud, J.K. Kochi. *J. Am. Chem. Soc.*, **108**, 2309 (1986).

[10] (a) D. Chatterjee, A. Mitra, B.C. Roy. *J. Mol. Catal., A: Chem.*, **161**, 17 (2000); (b) E.C. Samsel, K. Srinivasan, J.K. Kochi. *J. Am. Chem. Soc.*, **107**, 7606 (1985).

[11] (a) M. Wang, L.F. Wang, Y.Z. Li, Q.X. Li, Z.D. Xu, D.M. Qu. *Transition Met. Chem.*, **26**, 307 (2001); (b) L.D.S. Yadav, S. Singh. *Indian J. Chem.*, **40B**, 440 (2001); (c) A. Jarrahpour, D. Khalili, E. De Clercq, C. Salmi, J.M. Brunel. *Molecules*, **12**, 1720 (2007).

[12] Z. Cimerman, N. Galic, B. Bosner. *Anal. Chim. Acta*, **343**, 145 (1997).

[13] (a) R.K. Parashar, R.C. Sharma, A. Kumar, G. Mohan. *Inorg. Chim. Acta*, **151**, 201 (1988); (b) D.W. Robertson, E.E. Beedle, J.H. Krushinski, G.D. Pollock, H. Wilson, V.L. Wyss, J.S. Hayes. *J. Med. Chem.*, **28**, 717 (1985).

[14] (a) A. Ourari, L. Baameur, G. Bouet, M.A. Khan. *Electrochem. Commun.*, **10**, 1736 (2008); (b) A. Ourari, M. Khelafi, D. Aggoun, G. Bouet, M.A. Khan. *Adv. Phys. Chem.*, (2011) doi:10.1155/2011/157484; (c) A. Ourari, M. Khelafi, D. Aggoun, A. Jutand, C. Amatore. *Electrochim. Acta*, **75**, 366 (2012).

[15] M.C. Burla, R. Caliandro, M. Camalli, B. Carrozzini, G.L. Cascarano, L. De Caro, C. Giacovazzo, G. Polidori, R. Spagna. *J. Appl. Cryst.*, **38**, 381 (2005).

[16] G.M. Sheldrick. *SHELX97 – Program for Crystal Structure Analysis (Release 97 2)*, Göttingen (1998); (b) Bruker-AXS. *SAINT and SADABS*, Bruker Analytical X-ray Systems Inc., Madison, WI (2009).

[17] A. Ourari, K. Ouari, W. Moumeni, L. Sibous, G. Bouet, M.A. Khan. *Transition Met. Chem.*, **31**, 169 (2006).

[18] R.M. Silverstein, F.X. Webster. In *Spectrometric Identification of Organic Compounds*, 6th edn, pp. 34–35, John Wiley and Sons, New York (1999).

[19] S.R. Kelode, P.R. Mandlik. *J. Chem. Pharm. Res.*, **4**, 3368 (2012).
[20] P. Gili, M.G. Martin Reyes, P. Martin Zarza, I.L.F. Machado, M.F.C. Guedes da Silva, M.A.N.D.A. Lemos, A.J.L. Pombiero. *Inorg. Chim. Acta*, **244**, 25 (1996).
[21] P. Gili, M.G. Martin Reyes, P. Martin Zarza, M.F.C. Guedes da Silva, Y.-Y. Tong, A.J.L. Pombeiro. *Inorg. Chim. Acta*, **255**, 279 (1997).
[22] E.B. Seena, M.R. Prathapachandra Kurup. *Spectrochim. Acta, Part A*, **69**, 726 (2008).
[23] H. Temel, S. Ilhan, M. Sekerci. *Synth. React. Inorg. Met. Org. Chem.*, **32**, 1625 (2002).
[24] A. Böttcher, T. Takeuchi, K.I. Hardcastle, T.J. Meade, H.B. Gray. *Inorg. Chem.*, **36**, 2498 (1997).
[25] C. Rimington. *Biochem. J.*, **75**, 620 (1960).
[26] Z. Smekal, F. Brezina, Z. Sindelar, R. Klika. *Polyhedron*, **15**, 1971 (1996) (b) Y.L. Zhang, W.J. Ruan, X.J. Zhao, H.J. Wang, Z.A. Zhu. *Polyhedron*, **22**, 1535 (2003).
[27] S. Ilhan, H. Temel, I. Yilmaz, M. Sekerci. *J. Organomet. Chem.*, **692**, 3855 (2007).
[28] S. Ilhan, H. Temel, I. Yilmaz, M. Sekerci. *Polyhedron*, **26**, 2795 (2007).
[29] A.D. Kulkarni, S.A. Patel, P.S. Badami. *Int. J. Electrochem. Sci.*, **4**, 717 (2009).
[30] R.S. Nicholson, I. Shain. *Anal. Chem.*, **36**, 706 (1964).
[31] A.N. Golikand, J. Raoof, M. Baghayeri, M. Asgari, L. Irannejad. *Russ. J. Electrochem.*, **45**, 192 (2009).
[32] S.M. Golabi, A. Nozad. *Electroanalysis*, **16**, 199 (2004).
[33] R. Ojani, J.B. Raoof, S.R.H. Zavvarmahalleh. *Electrochim. Acta*, **53**, 2402 (2008).
[34] A.N. Golikand, M. Asgari, M.G. Maragheh, S. Shahrokhian. *J. Electroanal. Chem.*, **58**, 155 (2006).
[35] A.N. Golikand, J. Raoof, M. Baghayeri, M. Asgari, L. Irannejad. *Russ. J. Electrochem.*, **45**, 192 (2009).
[36] J. Losada, I. del Peso, L. Beyer. *J. Electroanal. Chem.*, **447**, 147 (1998).
[37] M.G. Bhowon, H.L.K. Wah, R. Narain. *Polyhedron*, **18**, 341 (1999).
[38] M. Bagherzadeh, M. Amini. *J. Coord. Chem.*, **63**, 3849 (2010).
[39] R. Rajarao, T.H. Kim, B.R. Bhat. *J. Coord. Chem.*, **65**, 2671 (2012).
[40] A. Nozad Golikand, M. Ghannadi Maragheh, L. Irannejad, M. Asgari. *Russ. J. Electrochem.*, **42**, 167 (2006).
[41] A. Vijayaraj, R. Prabu, R. Suresh, C. Sivaraj, N. Raaman, V. Narayanan. *J. Coord. Chem.*, **64**, 637 (2011).
[42] R. Saha, A. Ghosh, B. Saha. *J. Coord. Chem.*, **64**, 3729 (2011).
[43] S. Torres, G. Ferraudi, N.P. Chandıa, B. Matsuhiro. *J. Coord. Chem.*, **64**, 377 (2011).
[44] S. Jameh-Bozorghi, H. Esfandiari, H. Saravani, F.R. Charati, B.W. Skelton, M. Makha. *J. Coord. Chem.*, **65**, 994 (2012).
[45] Z. Nadealian, V. Mirkhani, B. Yadollahi, M. Moghadam, S. Tangestaninejad, I. Mohammadpoor-Baltork. *J. Coord. Chem.*, **65**, 1071 (2012).
[46] A.G.F. Shoair. *J. Coord. Chem.*, **65**, 3511 (2012).
[47] P. Guo, K.Y. Wong. *Electrochem. Commun.*, **1**, 559 (1999).